Cartesian convection driven dynamos at low Ekman number

Stephan Stellmach* and Ulrich Hansen
Institut für Geophysik, WWU Münster, Corrensstrasse 24, D-48149 Münster, Germany
(Received 5 December 2004; revised manuscript received 18 May 2004; published 23 November 2004)

The Cartesian dynamo model of Childress and Soward [Phys. Rev. Lett. **29**, 837 (1972)] is studied numerically in the regime of low viscosity. Dynamos with Ekman numbers E in the range $10^{-4} \geqslant E \geqslant 5\times10^{-7}$ are discussed and compared with the corresponding nonmagnetic states and with results obtained for imposed magnetic fields. We find that in the range of investigated Ekman numbers, a transition occurs from a flow regime where the planform of convection is only weakly affected by the dynamo generated field to a regime where the typical length scales of the flow are largely controlled by the Lorentz forces. The magnetic field acts to facilitate convection and leads to an increase in both the heat transport and in the amplitude of the flow. We demonstrate that this convection promoting effect allows for dynamo action even for Rayleigh numbers below the critical Rayleigh number for the onset of nonmagnetic convection.

DOI: 10.1103/PhysRevE.70.056312 PACS number(s): 47.65.+a, 91.25.Cw

I. INTRODUCTION

During the past decade, numerical modeling of fully three dimensional dynamo processes in spherical geometry has become an integral part of geomagnetic research. The results of these efforts are quite encouraging. The fields predicted by numerical models have the correct strength and their morphology at the Earth's surface closely resembles characteristics of geomagnetic data [1,2]. Moreover, field reversals have been found [3] and the underlying mechanisms are now analyzed in detail by using self-consistent dynamo models [4,5].

The main problem faced today is that although the output of the models is in good agreement with the observed fields, the dynamical regimes which are accessible to numerical investigations deviate considerably from what is expected for the Earth's core. Especially the low values of viscosity and of thermal and chemical diffusivities in the core pose difficulties which have not been overcome yet.

A dimensionless parameter used to indicate the strength of viscous effects is the Ekman number $E=\nu/(2\Omega L^2)$ defined as the ratio of the rotational time scale to the time scale of viscous diffusion. Here, ν denotes kinematic viscosity, Ω is angular velocity, and L denotes the core radius. A common estimate based on molecular viscosity is $E=O(10^{-15})$ in the Earth's core. Taking into account this very small value, it would be highly desirable to neglect viscous friction at all in the bulk of the core by assuming $E=0$, perhaps retaining viscous effects only in small boundary layers. Up until now all attempts to numerically model such a self-consistent magnetostrophic dynamo failed due to numerical instabilities (see e.g., Ref. [6]). For this reason, all self-consistent models have to rely on the stabilizing effect of viscous friction and the strategy is to reduce the Ekman number as far as possible. Unfortunately, the Ekman numbers achievable by numerical simulation exceed the estimated value for the Earth's core by many orders of magnitude. This overestimation of viscous effects leads to force balances and thus to dynamical regimes which probably deviate considerable from the conditions inside the Earth's core.

The idea of this study is to use a fully self-consistent model of the plane layer dynamo originally proposed by Childress and Soward [7] to investigate the system behavior at low Ekman number. Typically, spherical models today are able to reach $E=O(10^{-4})$ if all diffusion operators are retained in the classical form. The simpler Cartesian geometry allows us to study dynamos with Ekman numbers as low as $E=5\times10^{-7}$. Several groups used so-called hyperdiffusivities to get to comparable Ekman numbers in spherical geometry at least for the large scales. Usually the diffusivities (and thus E) are then assumed to be a rapidly increasing function of the wave number of the solution, effectively damping out high wave-number components. Hyperdiffusion is meant to represent transport processes at the subgrid scale but its appropriateness has been called into question [8,9]. For this reason we do not use any form of hyperdiffusion and retain classical viscous friction.

The low value of the Ekman number in our calculation allows us to investigate effects which are absent for moderate E and are thus not present in most of todays spherical numerical dynamo solutions. Special attention is paid to the influence of the dynamo generated magnetic field on the planform and amplitude of convection. For moderate Ekman numbers, dynamo solutions are strongly influenced by viscous friction. This usually prevents drastic changes of the flow in response to the generated magnetic field. In the low Ekman number case considered here, the viscous force can become of secondary importance in comparison to the Lorentz force and the convective flow is thus strongly controlled by the forces exerted by the magnetic field.

II. MODEL AND METHODS

A. Governing equations and boundary conditions

Thermal convection and magnetic field generation is studied in a rotating plane layer. An electrically conducting Boussinesq fluid confined between parallel walls at $z=0$ and

*Electronic address: stellma@earth.uni-muenster.de

$z=1$ is heated from below. The system rotates about the vertical axes with constant angular velocity.

The governing equations can be written in the form

$$\frac{E}{q\mathrm{Pr}}(\partial_t \mathbf{u} + \mathbf{u}\cdot\boldsymbol{\nabla}\mathbf{u}) - \mathbf{B}\cdot\boldsymbol{\nabla}\mathbf{B} = E\nabla^2\mathbf{u} - \boldsymbol{\nabla}\Pi - \hat{\mathbf{z}}\times\mathbf{u} + q\mathrm{Ra}T\hat{\mathbf{z}}, \quad (1)$$

$$\partial_t \mathbf{B} + \mathbf{u}\cdot\boldsymbol{\nabla}\mathbf{B} - \mathbf{B}\cdot\boldsymbol{\nabla}\mathbf{u} = \nabla^2\mathbf{B}, \quad (2)$$

$$\partial_t T + \mathbf{u}\cdot\boldsymbol{\nabla}T = q\nabla^2 T, \quad (3)$$

$$\boldsymbol{\nabla}\cdot\mathbf{u} = 0, \quad (4)$$

$$\boldsymbol{\nabla}\cdot\mathbf{B} = 0. \quad (5)$$

In Eqs. (1)–(5), the Prandtl number Pr, the Ekman number E, the modified Rayleigh number Ra, and the Roberts number q are defined by

$$E = \frac{\nu}{2\Omega L^2},\ \mathrm{Ra} = \frac{\alpha\Delta T g L}{2\Omega\kappa},\ q = \frac{\kappa}{\eta},\ \mathrm{Pr} = \frac{\nu}{\kappa}, \quad (6)$$

where η is magnetic diffusivity, Ω is angular velocity, g is gravitational acceleration, L is a typical length of the system, ν is kinematic viscosity, α denotes the thermal-expansion coefficient, κ the thermal diffusivity, and ΔT the applied temperature difference which drives the flow. The equations have been nondimensionalized by using L^2/η as the time scale, L as length scale, η/L as velocity scale, $(2\Omega\mu_0\rho\eta)^{1/2}$ as magnetic-field strength scale, and ΔT as temperature scale. ρ denotes density and μ_0 is the permeability of free space. In the following, we refer to the quantity $\mathrm{Ro} := E(q\mathrm{Pr})^{-1} = \eta/(2\Omega L^2)$ as the magnetic Rossby number. To simplify the notation, we further define

$$\widetilde{R} := \frac{\mathrm{Ra} - \mathrm{Ra}_c}{\mathrm{Ra}_c}, \quad (7)$$

where Ra_c is the critical Rayleigh number for the onset of nonmagnetic convection predicted by linear stability theory (see Sec. III A).

We assume that the horizonal boundaries are stress free, electrically perfectly conducting, and isothermal. In mathematical form, the boundary conditions are then given by

$$\frac{\partial u_{x,y}}{\partial z} = u_z = 0 \text{ at } z = \{0,1\}, \quad (8)$$

$$\frac{\partial B_{x,y}}{\partial z} = B_z = 0 \text{ at } z = \{0,1\}, \quad (9)$$

and

$$T(z=0) = 1,\ T(z=1) = 0. \quad (10)$$

The choice of stress free boundary conditions avoids the dynamical effect of Ekman boundary layers, whereas the perfectly conducting boundary condition facilitates comparison with theoretical studies of the plane layer dynamo.

To address the problem numerically, we restrict ourself to horizontally periodic solutions $\Phi(x,y,z) = \Phi(x+\Gamma i, y+\Gamma j, z)\ \forall\, i,j \in \mathbb{Z},\ x,y \in \mathbb{R},\ z \in [0,1],\ \Phi \in \{\mathbf{u},\mathbf{B},T\}$ where $\Gamma \in \mathbb{R}$ denotes the aspect ratio. Certainly, long wavelength structures are excluded by such a procedure and this may have dynamical consequences. Nevertheless, we hope that our solutions retain the basic characteristics of the full problem.

B. Useful definitions

For future reference we define the horizontal and volume averages

$$\langle\cdots\rangle_{xy} := \Gamma^{-2}\int_{[0,\Gamma]}\int_{[0,\Gamma]}\cdots dxdy,$$

$$\langle\cdots\rangle_{\mathcal{V}} := \Gamma^{-2}\int_{\mathcal{V}}\cdots dV,$$

where $\mathcal{V} := [0,\Gamma]\times[0,\Gamma]\times[0,1]$ is the computational domain. The time average is denoted by $\langle\cdots\rangle$. We further define

(a) the magnetic Reynolds number $\mathrm{Re}_m := \sqrt{\langle\mathbf{u}^2\rangle_{\mathcal{V}}}$,

(b) the Peclet number $\mathrm{Pe} := \mathrm{Re}_m/q$,

(c) the Reynolds number $\mathrm{Re} := \mathrm{Re}_m/(q\mathrm{Pr})$,

(d) the Elsasser number $\Lambda := \langle\mathbf{B}^2\rangle_{\mathcal{V}}$,

(e) the ratio of magnetic to kinetic energy

$$E_{mag}/E_{kin} := \mathrm{Ro}^{-1}\Lambda/\mathrm{Re}_m^2,$$

(f) the kinetic helicity $H := \sqrt{\langle(\mathbf{u}\cdot\nabla\times\mathbf{u})^2\rangle_{\mathcal{V}}}$,

(g) the Nusselt number $\mathrm{Nu} := \langle q^{-1}u_z T - \partial T/\partial z\rangle_{\mathcal{V}}$,

(h) a dimensionless measure for the deviation from a Taylor state

$$\tau := \left\langle \frac{\int_0^1 \hat{\mathbf{z}}\cdot\boldsymbol{\nabla}\times(\mathbf{B}\cdot\boldsymbol{\nabla}\mathbf{B})dz}{\int_0^1 |\hat{\mathbf{z}}\cdot\boldsymbol{\nabla}\times(\mathbf{B}\cdot\boldsymbol{\nabla}\mathbf{B})|dz}\right\rangle_{xy},$$

(i) and the number of free decay times $t_\eta := \pi^2\Delta t$.

The definition of τ is motivated in Sec. III B. t_η expresses the length of a calculated time series Δt in units of the free decay time of the slowest decaying mode.

Spectra of the solutions will be discussed in the next sections. We therefore expand $\mathbf{u}$ according to

$$\mathbf{u} := \sum_{l,m,n}\exp[2\pi i(lx+my)/\Gamma]\begin{pmatrix} u_{x_{l,m,n}}\cos(n\pi z)\\ u_{y_{l,m,n}}\cos(n\pi z)\\ u_{z_{l,m,n}}\sin(n\pi z)\end{pmatrix}, \quad (11)$$

where l, m are the horizontal wave numbers, n is the vertical wave number, and we define $k^2 := l^2+m^2$. A similar expression is used for $\mathbf{B}$ with fourier coefficients $\mathbf{B}_{l,m,n}$. To analyze the horizontal structure of the solution, we further define

$$v^2(l,m) = \sum_n E_{kin}(l,m,n), \quad (12)$$

$$\Lambda(l,m) = \sum_n E_{mag}(l,m,n), \tag{13}$$

where $E_{kin}(l,m,n) := (1/2q^2)[\mathbf{u}_{l,m,n}\mathbf{u}^*_{l,m,n}(1+\delta_{0n})]$ and $E_{mag}(l,m,n) := \frac{1}{2}[\mathbf{B}_{l,m,n}\mathbf{B}^*_{l,m,n}(1+\delta_{0n})]$ denote the contributions of the (l,m,n) mode to the dimensionless kinetic energy $\langle u^2\rangle_{\mathcal{V}}$ and magnetic energy $\langle B^2\rangle_{\mathcal{V}}$.

C. Numerical method

Dynamo calculations at low E are numerically challenging because of the small length scale $\mathcal{L}=O(E^{1/3})$ that naturally arises when the magnetic field is weak and because of the different time scales present in the dynamo problem. On the one hand, in order to get relevant statistics, the simulations have to cover several magnetic decay times, on the other hand, the time scales of magnetohydrodynamic waves decreases rapidly with decreasing E [6,10].

Differently from the usually applied spectral methods [11], we therefore choose a conservative second order finite volume discretization in space that allows for efficient parallelization using a three dimensional domain decomposition approach [12]. Details of the method are given in Ref. [13], so we only give a brief summary here. A similar approach has also recently been applied to the spherical problem [14].

A primitive variable formulation is used in contrast to the commonly employed formulation in terms of poloidal and toroidal potentials (see, e.g., Ref. [2]). To allow a straightforward treatment of the Coriolis term, a collocated grid is used. Flux vector splitting is applied to the convective terms which transforms them into Elsasser space [15]. Second order upwind discretization by the QUICK scheme [16] is then used to avoid artificial hyperbolic behavior.

The stiffness is dealt with by using a fully implicit second order BDF time stepping scheme [17] which is not limited by the severe restrictions of the time step length typical for explicit methods (see, e.g., Ref. [18]). The time derivative is approximated as

$$\partial_t\phi = \alpha_0\phi^{n+1} + \alpha_1\phi^n + \alpha_2\phi^{n-1}, \tag{14}$$

with

$$\alpha_0 = \frac{1}{\Delta t}\frac{1+2\delta}{1+\delta},\ \alpha_1 = -\frac{1}{\Delta t}(1+\delta),\ \alpha_2 = \frac{1}{\Delta t}\frac{\delta^2}{1+\delta}, \tag{15}$$

where $\Delta t = t^{n+1}-t^n$, $\delta = \Delta t/(t^n - t^{n-1})$ and the superscripts denote time levels. To solve the resulting system of nonlinear equations, we basically follow the SIMPLE algorithm [19]. The pressure equation is solved by the Krylov subspace method BICGSTAB [20]. After each time step, the magnetic field is corrected in order to fulfill the solenoidal condition (5).

D. Modeling strategy

The parameters have been chosen with the intention to reduce the Ekman number as far as possible. We thus confine this study to Rayleigh numbers close to the critical Rayleigh number Ra_c for the onset of nonmagnetic convection. Apart from easing the computations, this has the advantage that the gross characteristics of nonmagnetic convection can still be understood in terms of weakly nonlinear theory.

TABLE I. Parameter values for nonmagnetic calculations.

E	1×10^{-4}	5×10^{-5}	2.5×10^{-5}	1×10^{-5}	5×10^{-6}
Ra	223.45	280.25	352.03	477.12	600.0
Pr	1	1	1	1	1
Grid	64^3	96^3	96^3	128^3	$256^2\times128$

The main concern of this paper is the study of dynamos at low E. Of particular importance in this context is to understand in which way a self-generated magnetic field influences the convective flow. We therefore start by investigating the nonmagnetic problem in Sec. III A. We then examine the transition of the flow regime that occurs when a magnetic field is imposed externally on the convective flow in Sec. III B. Finally, the full dynamo problem is studied in Sec. III C. The results gained for the nonmagnetic case on the one hand and for the case of a strong imposed field on the other hand serve as extreme cases against which the self-consistent dynamos can be compared.

III. RESULTS

A. Nonmagnetic convection

Linear theory predicts the critical Rayleigh number Ra_c and wave number k_c for the onset of convection to scale as $E^{-1/3}$ [22]. For $\mathrm{Pr} > 0.68\ldots$, convection sets in as stationary convection. We exclusively consider this case in the present paper.

The results of linear theory can be illustrated by considering the z component of the vorticity equation

$$\mathrm{Ro}(\partial_t\boldsymbol{\omega} + \mathbf{u}\cdot\boldsymbol{\nabla}\boldsymbol{\omega} - \boldsymbol{\omega}\cdot\boldsymbol{\nabla}\mathbf{u}) - E\nabla^2\boldsymbol{\omega} = \partial_z\mathbf{u} + q\mathrm{Ra}\,\boldsymbol{\nabla}\times(T\hat{\mathbf{z}}), \tag{16}$$

where $\boldsymbol{\omega} := \boldsymbol{\nabla}\times\mathbf{u}$ denotes the vorticity. It follows that convection can only occur (i.e., $\partial_z u_z \neq 0$) if either inertial or viscous forces balance the nonconservative part of the Coriolis force. For the considered Prandtl numbers, the viscous force breaks the rotational constraint. The scaling $k = O(E^{-1/3})$ follows directly from Eq. (16) as long as $\partial_z u_z = O(1)$ and is thus expected to be a robust feature even for high flow amplitudes.

1. Choice of parameter values

Table I shows the employed parameter values. The Ekman number is varied in the range $5\times10^{-6} \leqslant E \leqslant 10^{-4}$. The Prandtl number is fixed to one and we have chosen the Rayleigh number such that $\widetilde{R} = (\mathrm{Ra}-\mathrm{Ra}_c)/\mathrm{Ra}_c$ is constant for all Ekman numbers considered. Since the Roberts number q is not a relevant control parameter in the nonmagnetic case, we assume $q=1$ in the following. The nondimensional time scale is then the thermal diffusion time and the velocity scaling is based on the local Peclet number.

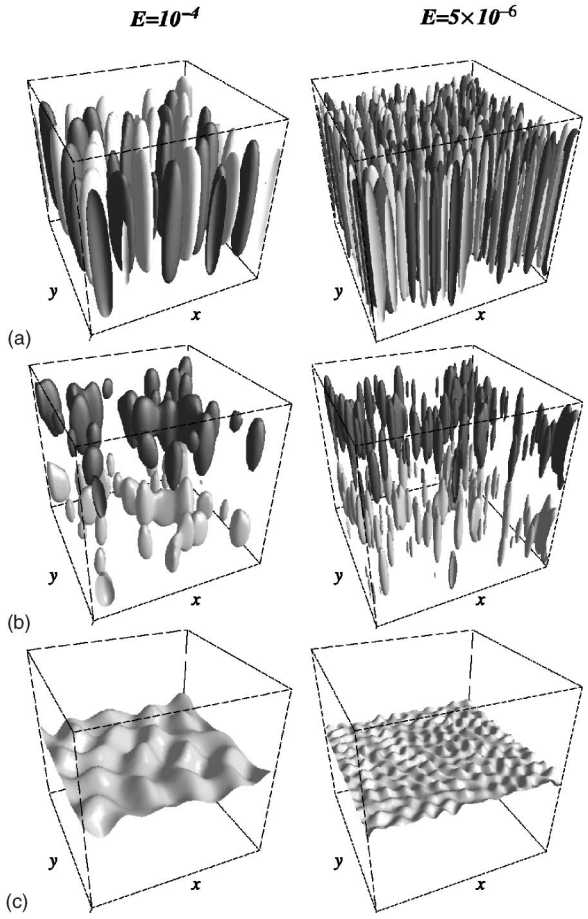

FIG. 1. Visualizations of the flow structures for nonmagnetic convection at $E=10^{-4}$ (left column) and at $E=5\times10^{-6}$ (right column). The panels in the top row (a) shows isosurfaces of u_z at $u_z=\pm30$ for $E=10^{-4}$ and at $u_z=\pm50$ for $E=5\times10^{-6}$ (upstreams: dark gray; downstreams: light gray). A snapshot of the spatial distribution of helicity is shown in (b) at 50% (light gray) and −50% (dark gray) of the maximum absolute value. The plots in the lowermost row (c) show temperature isosurfaces at $T=0.5$.

2. Flow structure

For all parameter values considered, the flow exhibits a chaotic time dependence. To give an impression of the spatial structure of the flow, snapshots are shown in Fig. 1 for $E=10^{-4}$ (left column) and for $E=5\times10^{-6}$ (right column). The top row (a) shows the geometry of the up- and downstreams by means of isosurfaces of the vertical velocity. The flow has a columnar structure and the typical size of the convection columns strongly decreases with decreasing E. The kinetic helicity exhibits a strong polarization along the z axes (Ref. [21], Chap. 8.2) with positive helicity dominating in the lower and negative helicity in the upper half of the fluid layer. This is visualized by isosurfaces of $\mathbf{u}\cdot\boldsymbol{\nabla}\times\mathbf{u}$ in the second row (b). The spatial helicity polarization is crucial for the ability of the flow to act as a kinematic dynamo. Isosurfaces of temperature are shown in the last row of Fig. 1. Due to the moderately supercritical value of Ra, the deviations of the temperature from the purely conductive gradient are small and there are no thermal boundary layers as typical for high Rayleigh number convection. The temperature isosurfaces are almost flat and only slightly deformed by the convective heat transport in the up- and downstreams.

For a more quantitative description the spectral distribution of kinetic energy has been calculated. Figure 2 shows the time average of the quantity $v^2(l,m)$ defined in Sec. II B. The most prominent feature is pronounced maxima at wave numbers close to the critical wave number k_c as obtained from linear theory. For $\Gamma=1$, these are $k_c=\sqrt{20}\approx4.47$ for $E=10^{-4}$ and $k_c=\sqrt{148}\approx12.17$ for $E=5\times10^{-6}$ [22]. There is thus a clear preferred length scale of order $E^{1/3}$ of the flow structures even in the finite amplitude case.

3. Ekman number scalings

The relative amount by which the Rayleigh number exceeds its critical value determines the strength of the convective heat transport. In the chosen case of constant $\tilde{R}$, the Nusselt number Nu is almost constant, independently of the Ekman number (see Table II). Differently, the flow amplitude does not remain constant, but increases with decreasing Ekman number. Figure 3 shows the scaling of Re and H with E. The Reynolds number scales approximately as $\mathrm{Re}\propto E^{-1/3}$. Since the dominating length scales are $\mathcal{L}=O(E^{1/3})$, the helicity is expected to scale approximately as $\mathcal{L}^{-1}\mathcal{U}^2=O(E^{-1})$ and the results indeed reveal an approximate $1/E$ scaling.

These scaling exponents are still in good agreement with results from weakly nonlinear theory [23]. For moderately supercritical Rayleigh numbers, a statistically stationary finite amplitude state results from the reduction of the mean vertical temperature gradient in the interior of the fluid by

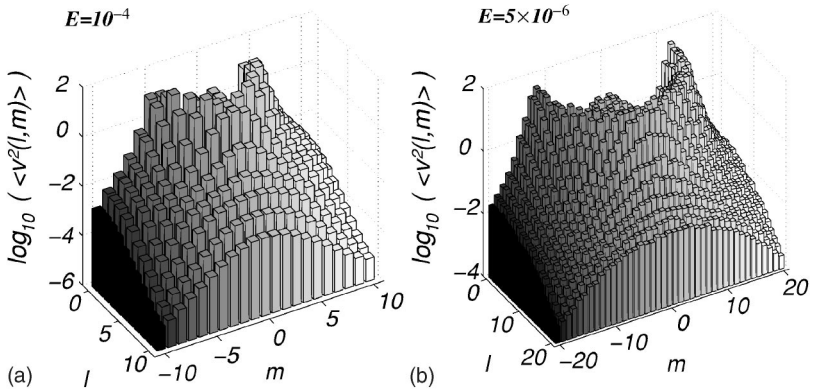

FIG. 2. Spectra of dimensionless kinetic energy for nonmagnetic convection at (a) $E=10^{-4}$ and (b) $E=5\times10^{-6}$.

TABLE II. Overview of the dynamo calculations. Re_m is the magnetic Reynolds number, Re is the Reynolds number, Nu is the Nusselt number, Λ is the Elsasser number, and E_{mag}/E_{kin} is the magnetic to kinetic energy ratio. The values in parenthesis correspond to nonmagnetic convection. *Field and flow decayed after more than two mean field decay times. The values given are averages over the period of transient dynamo action.

Run	1	2	3	4	5	6	7	8*	9	10	11
E	1×10^{-4}	5×10^{-5}	2.5×10^{-5}	1×10^{-5}	5×10^{-6}	5×10^{-6}	5×10^{-6}	5×10^{-6}	5×10^{-6}	5×10^{-6}	5×10^{-7}
Ra	223.45	280.25	352.03	477.12	600.00	600.00	500.00	450.00	600.00	600.00	1200.00
Ra_c	189.71	237.93	298.88	405.07	509.40	509.40	509.40	509.40	509.40	509.40	1095.98
Pr	1	1	1	1	1	1	1	1	10	30	1
q	2.5	2.5	2.5	2.5	2.5	1	1	1	1	1	1
Γ	1	1	1	1	1	1	1	1	1	1	0.25
Grid	64^3	96^3	96^3	128^3	128^3	128^3	128^3	128^3	96^3	80^3	$64^2\times256$
t_η	12.22	5.51	4.23	2.64	2.10	2.59	7.84	2.05	4.81	4.07	1.95
Re_m	110.5	141.8	170.7	198.9	215.4	136.6	102.4	82.3	127.1	118.6	221.2
	(74.6)	(92.8)	(120.6)	(165.8)	(204.0)	(81.6)	(0.0)	(0.0)	(91.7)		(127.5)
Re	44.2	56.7	68.3	79.6	86.2	136.6	102.4	82.3	12.7	4.0	221.2
	(29.8)	(37.1)	(48.3)	(66.3)	(81.6)	(81.6)	(0.0)	(0.0)	(9.2)		(127.5)
Nu	1.71	1.73	1.66	1.49	1.37	1.91	1.63	1.47	1.62	1.54	1.84
	(1.32)	(1.32)	(1.34)	(1.35)	(1.33)	(1.33)	(1.0)	(1.0)	(1.38)		(1.20)
Λ	0.31	0.38	0.38	0.31	0.24	0.21	0.16	0.12	0.09	0.07	0.20
E_{mag}/E_{kin}	0.62	0.97	1.37	2.07	2.86	2.33	3.06	3.60	10.57	27.71	15.54

the convective heat transport. Since the horizontal length scales of the flow decrease with decreasing Ekman number, the flow velocities have to increase in order to achieve the necessary reduction of the vertical temperature gradient.

4. Summary of nonmagnetic results

In summary, we conclude that for the chosen Parameter values, all results share the same dynamical behavior. The scaling exponents found are in good agreement with those predicted by weakly nonlinear theory. These scaling laws are likely to hold in the limit $E\to0$ provided $\tilde{R}$ is chosen small enough to restrict the flow amplitude to values for which inertial effects are of secondary importance.

Furthermore, in Sec. III C, we show that the flow amplitudes are high enough to make kinematic dynamo action possible for order one Roberts numbers. The observed flow regime is thus an excellent starting point for the study of nonlinear dynamos.

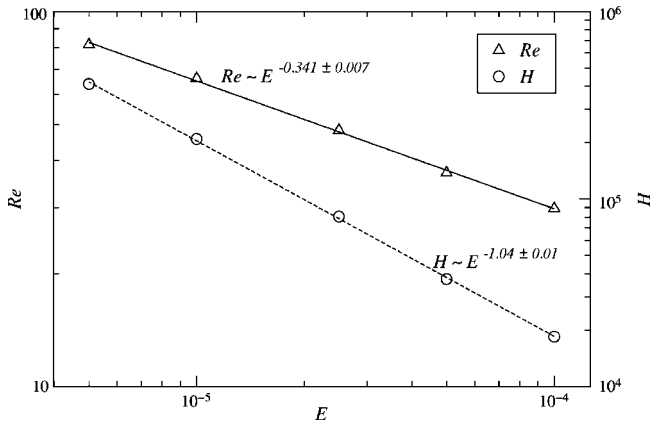

FIG. 3. Scaling of the time averaged helicity and Reynolds number for constant $\tilde{R}$ in the nonmagnetic case.

B. Magnetoconvection

After describing the main features of nonmagnetic convection, in this section we study the response of the convective flow to an externally applied magnetic field. Many ideas concerning the nonlinear dynamics governing the dynamo case are based on magnetoconvection studies. The results of this section will thus be useful in interpreting the self-consistent dynamo calculations in Sec. III C.

Most previous studies have been performed with a constant imposed field $\mathbf{B}_\perp=\sqrt{\Lambda_\perp}\hat{\mathbf{x}}$ of prescribed strength $\Lambda_\perp$. The linearized stability problem has been investigated for finite Prandtl number in the limit $E\to0$ [24,25] and for general, finite Ekman numbers in the infinite Prandtl number limit [26]. These works clearly demonstrate that for the small Ekman number case considered in this paper, k_c and Ra_c are both $O(1)$ independently from the Ekman number provided the field strength $\Lambda_\perp$ also exceeds an order one value.

This result of linear stability theory can again be illustrated by considering the vorticity equation

$$\mathrm{Ro}(\partial_t\boldsymbol{\omega}+\mathbf{u}\cdot\boldsymbol{\nabla}\boldsymbol{\omega}-\boldsymbol{\omega}\cdot\boldsymbol{\nabla}\mathbf{u})-E\nabla^2\boldsymbol{\omega}=\boldsymbol{\nabla}\times(\mathbf{B}\cdot\boldsymbol{\nabla}\mathbf{B})+\partial_z\mathbf{u}+q\mathrm{Ra}\,\boldsymbol{\nabla}\times(T\hat{\mathbf{z}}),\qquad(17)$$

where $\mathbf{B}=\mathbf{B}_\perp+\mathbf{b}$ denotes the magnetic field consisting of the imposed field $\mathbf{B}_\perp$ and of fluctuations $\mathbf{b}$ induced by the convective flow. Differently from the nonmagnetic case, the nonconservative part of the Coriolis force can now be balanced by the Lorentz force provided the imposed field is

strong enough. This liberates the system from the severe constraints imposed by rapid rotation. The dominating force balance is now between Coriolis, pressure, buoyancy, and Lorentz forces while viscosity plays a minor role and the need for the presence of a small length scale vanishes.

If the nonlinear problem is considered, complications arise in the limit $E \to 0$ because of the fact that the momentum equation (1) might not have any solutions for $E = \mathrm{Ro} = 0$. A necessary condition for the existence of solutions can be derived by integrating the z component of Eq. (17) from the bottom to the top boundary over z, yielding

$$\mathrm{Ro}\left(\partial_t \int_0^1 \omega_z dz + \int_0^1 \mathbf{u} \cdot \boldsymbol{\nabla}\, \omega_z dz - \int_0^1 \boldsymbol{\omega} \cdot \boldsymbol{\nabla}\, u_z dz \right) - E \int_0^1 \nabla^2 \omega_z dz = \int_0^1 \hat{\mathbf{z}} \cdot \boldsymbol{\nabla} \times (\mathbf{B} \cdot \boldsymbol{\nabla}\, \mathbf{B}) dz. \qquad (18)$$

In the magnetostrophic case $\mathrm{Ro} = E = 0$ this equation reduces to the desired solvability condition

$$\int_0^1 \hat{\mathbf{z}} \cdot \boldsymbol{\nabla} \times (\mathbf{B} \cdot \boldsymbol{\nabla}\, \mathbf{B}) dz = 0 \ \ \forall \ \ (x,y) \in \mathbb{R}^2, \qquad (19)$$

which represents Taylor's constraint in Cartesian geometry. The quantity τ defined in Sec. II B provides a measure of the degree to which Eq. (19) is satisfied in a numerical simulation [27].

Building up on the linear results, Roberts and Stewartson [28,29] studied the weakly nonlinear case. Complications arise for strong magnetic fields and moderate Roberts numbers. In this case, there is a degeneracy in the linear stability problem and two distinct rolls are equally possible. Their nonlinear interaction leads to a violation of Taylor's condition [29]. The resulting Lorentz force can then only be balanced by inertial forces resulting in a geostrophic flow $\mathbf{u}_g = u_g(y)\hat{\mathbf{x}}$ which plays a crucial role in the dynamics of the system. We found that in fully nonlinear calculations, $\mathbf{u}_g$ can become very strong if a simple, one dimensional mean field $\mathbf{B}_\perp = B_\perp(z)\hat{\mathbf{x}}$ is applied externally. To avoid this kind of behavior, a more complicated, two dimensional mean field is used in this study.

1. Governing equations

The governing equations are derived by separating the magnetic field into a mean part $\mathbf{B}_\perp = \langle \mathbf{B} \rangle_{xy}$ and a fluctuating part $\mathbf{b} := \mathbf{B} - \mathbf{B}_\perp$. The induction equation then becomes

$$\partial_t \mathbf{B}_\perp = -\langle \mathbf{u} \cdot \nabla\, \mathbf{b} - \mathbf{b} \cdot \nabla\, \mathbf{u} \rangle_{xy} + \nabla^2 \mathbf{B}_\perp, \qquad (20)$$

$$\partial_t \mathbf{b} = -\mathbf{u} \cdot \boldsymbol{\nabla}\, (\mathbf{B}_\perp + \mathbf{b}) + (\mathbf{B}_\perp + \mathbf{b}) \cdot \boldsymbol{\nabla}\, \mathbf{u} + \langle \mathbf{u} \cdot \nabla\, \mathbf{b} - \mathbf{b} \cdot \nabla\, \mathbf{u} \rangle_{xy} + \nabla^2 \mathbf{b}. \qquad (21)$$

Since at this stage we are interested only in the response of the system to an imposed mean field of given strength $\Lambda_\perp$, we neglect the process of mean field generation here, assume $\mathbf{B}_\perp$ to be given and solve Eq. (21) together with Eqs. (1), (3), and (4), and $\boldsymbol{\nabla} \cdot \mathbf{b} = 0$.

2. Choice of applied mean field

The applied mean field has been chosen to be as simple as possible. To be physically meaningful, it must satisfy the boundary conditions (9) and the condition $\int_0^1 \mathbf{B}_\perp dz = 0$. The simplest choice $\mathbf{B}_\perp = \sqrt{2\Lambda_\perp} \cos(\pi z)\hat{\mathbf{x}}$, however, rapidly leads to a strong geostrophic flow $\mathbf{u}_g = u_g(y)\hat{\mathbf{x}}$ [29] which is undesirable in this context. The inclusion of third order terms in the Fourier representation of $\mathbf{B}_\perp$,

$$\mathbf{B}_\perp = \sqrt{\Lambda_\perp} \begin{pmatrix} \sqrt{2}/2[\cos(\pi z) - \cos(3\pi z)] \\ -\cos(\pi z) \\ 0 \end{pmatrix}, \qquad (22)$$

eliminates this problem. The chosen field has a spiral staircase structure, is antisymmetric with respect to the midplane $z = 0.5$, and thus has at least some similarities with the fields observed in the dynamo case [Sec. III C and Fig. 10(c)]

3. Procedure and choice of parameters

To facilitate the comparison of the relevant flow regimes with the nonmagnetic case, the Rayleigh, Ekman, and Prandtl numbers are the same as for the nonmagnetic calculations (see Table I). For simplicity, we further assume $q = 1$ in this section resulting in the fact that all diffusive time scales are the same.

Two sets of numerical experiments have been performed. For fixed $E = 5 \times 10^{-6}$, $\Lambda_\perp$ has been systematically varied in the range $0 \leqslant \Lambda_\perp \leqslant 10$ to explore the response of the system to weak and strong imposed fields. We have further investigated the dependence of the strong field states at $\Lambda_\perp = 10$ on the Ekman number for $5 \times 10^{-6} \leqslant E \leqslant 10^{-4}$. A 64^3 grid has been used for all calculations.

4. Flow structure

Figure 4 shows the resulting flow structures at $E = 5 \times 10^{-6}$ for various values of the imposed field strength $\Lambda_\perp$. For small values of $\Lambda_\perp$, the flow is similar to the nonmagnetic case described in Sec. III A. and obeys the weak field scaling $\mathcal{L} \propto E^{1/3}$. The Taylor proudman theorem manifests itself in the close similarity of both temperature isosurfaces shown in Fig. 4(a). With increasing field strength $\Lambda_\perp$, the typical size of the flow structures increases and the Taylor proudman effect successively loses significance. For $\Lambda_\perp = 10$, the flow is dominated by large scale features of size $\mathcal{L} \propto O(1)$. We further observe that the temperature isosurfaces successively become closer to the boundary with increasing field strength. This reflects the fact that thermal boundary layer structures develop at large $\Lambda_\perp$.

5. Influence of the applied field strength

Figure 5 gives a more quantitative description of the effects of the imposed field on the convective flow. It shows the Reynolds number and the quantity τ defined in Sec. III B as a function of the applied field strength $\Lambda_\perp$. With increas-

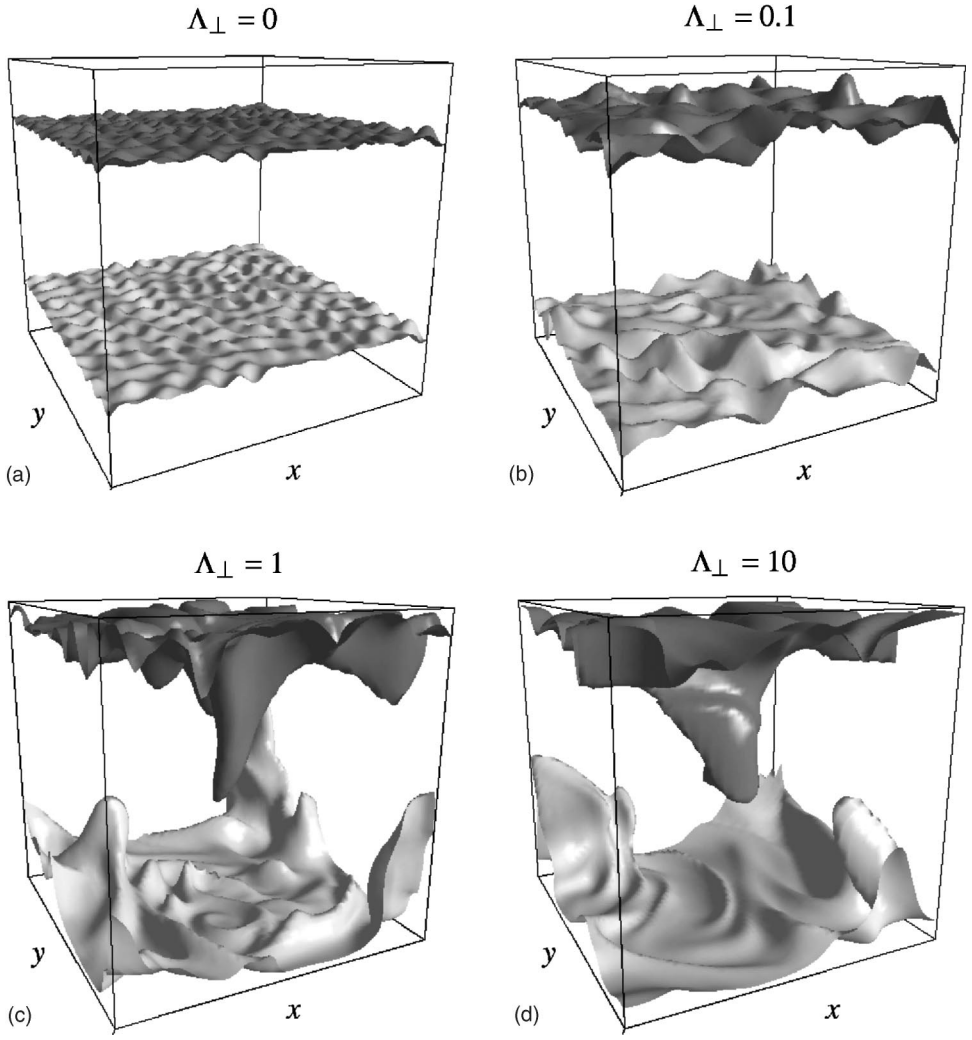

FIG. 4. Isosurfaces of temperature at $T=0.3$ and at $T=0.7$ for various values of the imposed field strength in the magnetoconvection case ($E=5\times10^{-6}$, Ra$=600$, Pr$=q=1$).

ing $\Lambda_\perp$, the amplitude of the flow as measured by the Reynolds number strongly increases. This is to be expected on the grounds of linear theory since for $\Lambda_\perp \leqslant O(1)$, the system gets increasingly supercritical with increasing $\Lambda_\perp$. We further observe that τ rapidly decreases in the range $0.1 \leqslant \Lambda_\perp \leqslant 1$ and that a transition to an approximate Taylor state, characterized by a value of τ much smaller than one, occurs.

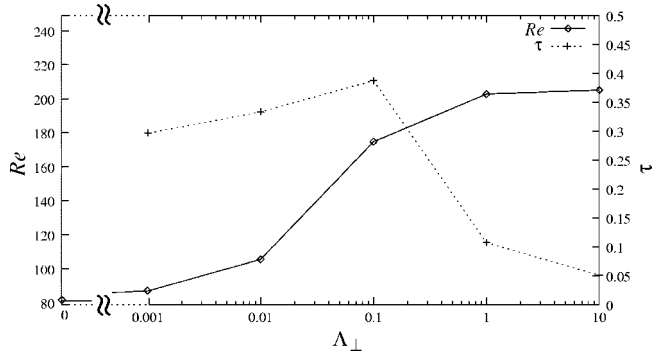

FIG. 5. Reynolds number and τ as a function of the imposed field strength for $E=5\times10^{-6}$, Ra$=600$, and Pr$=q=1$).

6. Ekman number scalings

We further computed the Ekman number dependence of the strong field states with $\Lambda_\perp=10$. These might be contrasted with the weak field scaling laws discussed in Sec. III A. Figure 6(a) shows the convective heat transport (measured by the Nusselt number) and the Reynolds number as a function of E.

As compared to nonmagnetic convection, the heat transport across the fluid layer is much higher in the magnetoconvection case. This is caused by the fact that large scale convection is much more efficient in transporting heat than the small scale flows arising in the nonmagnetic case. In addition, for fixed $\widetilde{R}$ the Nusselt number now increases with decreasing Ekman number. This is due to the system becoming more and more supercritical with decreasing E. A power-law fit results in the approximate scaling $\mathrm{Nu} \propto E^{-1/5}$.

The amplitude of the convection as measured by the Reynolds number also increases with decreasing E. In this case, a power-law fit results in $\mathrm{Re} \propto E^{-0.29}$. Note that in the magnetoconvection case considered here Re increases slower with decreasing E than for nonmagnetic convection. At first

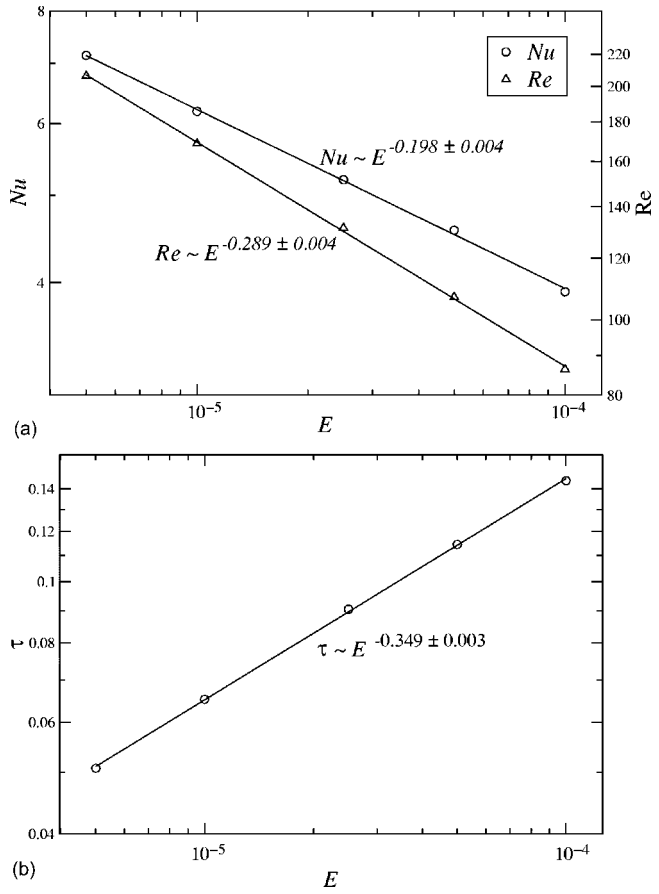

FIG. 6. Ekman number dependence for an imposed field strength $\Lambda_\perp = 10$. (a) shows Nu and Re as a function of E and (b) displays the Ekman number dependence of τ.

glance, this suggests that for fixed $\widetilde{R}$ and decreasing Ekman number, nonmagnetic convection ultimately becomes more vigorous than magnetoconvection. The corresponding Reynolds numbers however become so large that the scaling laws discussed here are likely to lose validity.

Figure 6(b) shows the Ekman number dependence of τ at $\Lambda_\perp = 10$. With decreasing Ekman number, the influence of viscosity is reduced and the magnetic field satisfies Taylor's condition increasingly well. We find that τ scales approximately as $\tau \propto E^{-1/3}$.

7. Summary of magnetoconvection results

In summary, we conclude that the presence of a strong magnetic field fundamentally changes the dynamical regime from a viscously dominated to a magnetostrophic one. The influence of viscosity uniformly decreases with decreasing Ekman number. We further find that even for weak magnetic fields with an intensity too low to cause a transition to an approximate state, both the planform and the amplitude of convection strongly depend on the applied field strength.

The flow regimes found for either nonmagnetic convection and for strong imposed magnetic fields provide extreme cases which are helpful for the interpretation of dynamo calculations. In the self-consistent dynamo problem, the energy necessary to prevent the magnetic field from Ohmic decay must be provided by work done against Lorentz forces. This restriction is absent in the magnetoconvection problem where the large scale field is prescribed. Nevertheless, the convective flows are expected to be largely influenced by the magnetic field in the dynamo case at low Ekman number.

C. Dynamos

In Sec. III A we described the character of nonmagnetic convection. The Rayleigh numbers were chosen small enough for scaling laws predicted by weakly nonlinear analysis to hold. In this case, for constant $\widetilde{R}$ the Reynolds number scales according to $\mathrm{Re} \propto E^{-1/3}$ while the Nusselt number is almost constant. The convective flow is characterized by a preferred length scale of order $E^{1/3}$.

The effect of an imposed magnetic field on the amplitude and planform of convection was studied for the same set of control parameters in Sec. III B. We demonstrated that the presence of a strong magnetic field leads to a dynamical regime which is drastically different from the nonmagnetic case. The presence of the imposed field leads to large scale convection accompanied by very efficient heat transport and a nearly magnetostrophic force balance.

In this section we study the full dynamo problem in which the magnetic field is self-generated. According to the theoretical analysis of Soward [23], we would expect a weak initial magnetic field to be amplified by kinematic dynamo action provided the magnetic Reynolds number is high enough. This kinematic dynamo generates an oscillatory magnetic field by the typical two scale mechanism in which

(1) small scale field **b** is generated from the large scale mean field $\mathbf{B}_\perp$ by the small scale motions, and

(2) the large scale field $\mathbf{B}_\perp$ is induced by the average of the action of the small scale convective flow on the small scale field **b**.

Small scale motions are inefficient at generating magnetic field. Balancing terms in the dimensionless form of the induction equation, where the large length scale is assumed to be $O(1)$ suggests that the critical magnetic Reynolds number for the onset of dynamo action scales as $E^{-1/6}$ and this is also revealed by Soward's analysis of the kinematic dynamo problem [23]. In the nonmagnetic case we found $\mathrm{Re} \propto E^{-1/3}$ for fixed $\widetilde{R}$. We therefore expect that the marginal $\widetilde{R}$ for the onset of kinematic dynamo action decreases with decreasing E.

Soward studied the case of weak magnetic fields with $\Lambda = O(E)$ by means of an amplitude expansion. In this case, the leading order kinetic energy balance is not affected by the magnetic field and a dynamical equilibrium is possible provided $\widetilde{R}$ is small enough. In this regime, the Lorentz force only controls the fine structure of the flow which still has small horizontal length scales $\mathcal{L} = O(E^{1/3})$.

Subsequent analysis by Fautrelle and Childress [30] for intermediate field strength $\Lambda = O(E^{2/3})$ revealed that such fields lead to instability and rapid field growth occurs. This showed that the weak field solutions are very special in the sense that they are unstable to finite magnetic perturbations. The finding is consistent with results from magnetoconvec-

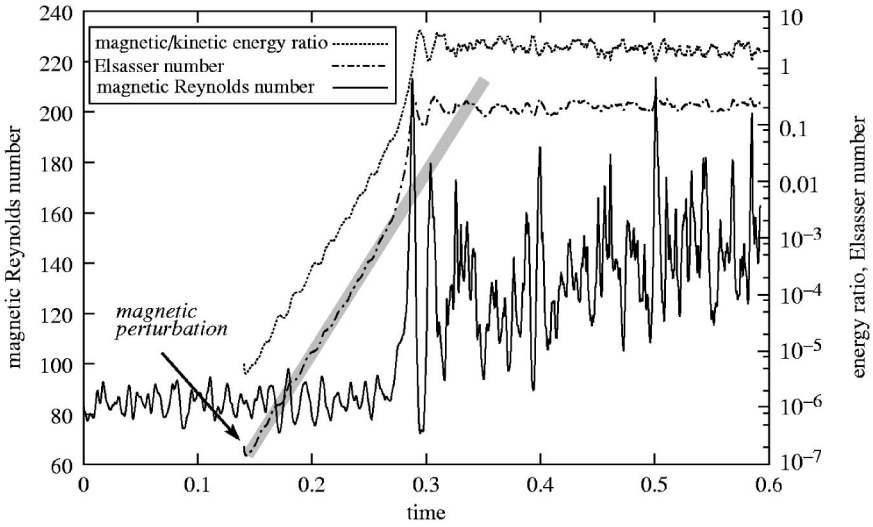

FIG. 7. Temporal evolution of the magnetic Reynolds number Re_m, the Elsasser number Λ, and the ratio of magnetic to kinetic energy E_{mag}/E_{kin} for $E=5\times10^{-6}$, Ra=600, Pr=q=1. The dynamo was started by inserting a small initial field into fully developed nonmagnetic convection. The gray bar indicates the phase of exponential kinematic growth.

tion theory for externally applied uniform fields which are known to reduce the critical Rayleigh number for the onset of convection and thus strongly facilitate convective motions. The analysis of the last section revealed that this convection promoting effect also occurs for nonuniform applied fields in the fully nonlinear case.

The so called "runaway" field growth described above is expected to continue until the Lorentz forces prevent further field amplification and a dynamical balance between Coriolis, Lorentz, buoyancy, and pressure forces is set up. Analytical studies in this regime are difficult since the convection is dominated by large scale features so that the two scale method is no longer applicable.

The scenario described above is derived from weakly nonlinear theory in the small Ekman number limit. In this section, we discuss results from fully nonlinear dynamo calculations at varying values of the Ekman number $5\times10^{-7}\leqslant E\leqslant10^{-4}$. We will demonstrate that transition takes place in this range from a viscously controlled regime to a state where the flow structure is largely influenced by the magnetic field.

1. Choice of parameters

Table II shows the values of the control parameters employed for the dynamo calculations. The parameter values used in Secs. III A and III B have been included to allow a comparison with the nonmagnetic and magnetoconvection results. A Roberts number $q=2.5$ has been chosen to permit kinematic dynamo action at $E=10^{-4}$ and the corresponding calculations at lower E also use this value of q. At low values of the Ekman number, the increase of the amplitude of convection with decreasing Ekman number allows kinematic dynamo action at lower Roberts numbers. Most calculations at low Ekman number thus apply $q=1$ which prevents the magnetic field from developing very small scales and at the same time reduces the numerical stiffness of the problem.

For $E<5\times10^{-6}$, the aspect ratio was reduced to $\Lambda=0.25$ to resolve the small horizontal length scale of nonmagnetic convection. This is no severe limitation for the nonmagnetic case since the box still contains many convection cells. It, however, clearly limits the size of the largest convection cells in the dynamo case.

2. Nonexponential field growth

Most of the dynamos discussed in this section have been obtained by using the output of runs at different parameter values as the initial condition. In some cases, the dynamos were started by inserting a small magnetic perturbation into statistically stationary nonmagnetic convection. This initial field is then amplified by the convective flow through kinematic dynamo action and initially the magnetic field grows exponentially with a well defined growth rate. As an example, Fig. 7 shows for $E=5\times10^{-6}$, Ra=600, Pr=q=1 the temporal evolution of Λ, R_m, and E_{mag}/E_{kin}. Eventually the magnetic field becomes strong enough to destabilize the convection which leads to increasing flow velocities. Figure 7 shows that this in turn causes more efficient dynamo action resulting in very fast, nonexponential field growth until saturation occurs.

The effect just described is observable in all our simulations in which the dynamo grows from a small initial field. It results from two instabilities (magnetic field intensification by induction and destabilization of the convective flow by the induced field) occurring at the same time. This "runaway field growth" is strongest at low E and in cases where the magnetic Reynolds number is close to the marginal value for the onset of dynamo action. The kinematic growth rate is then small and changes rather drastically when the magnetic field starts to destabilize convection. In addition, the flow velocities differ more strongly between the nonmagnetic and the saturated dynamo branch at small R_m.

3. Flow structure in the saturated regime

In the saturated regime, the influence of **B** on the planform of convection successively becomes more pronounced with decreasing Ekman number. Figure 8 contrasts time averaged kinetic energy spectra for the nonmagnetic and the dynamo case at three different Ekman numbers. For $E=10^{-4}$, the scales of the flow are nearly uninfluenced by the action of the magnetic field as revealed by the similarity of

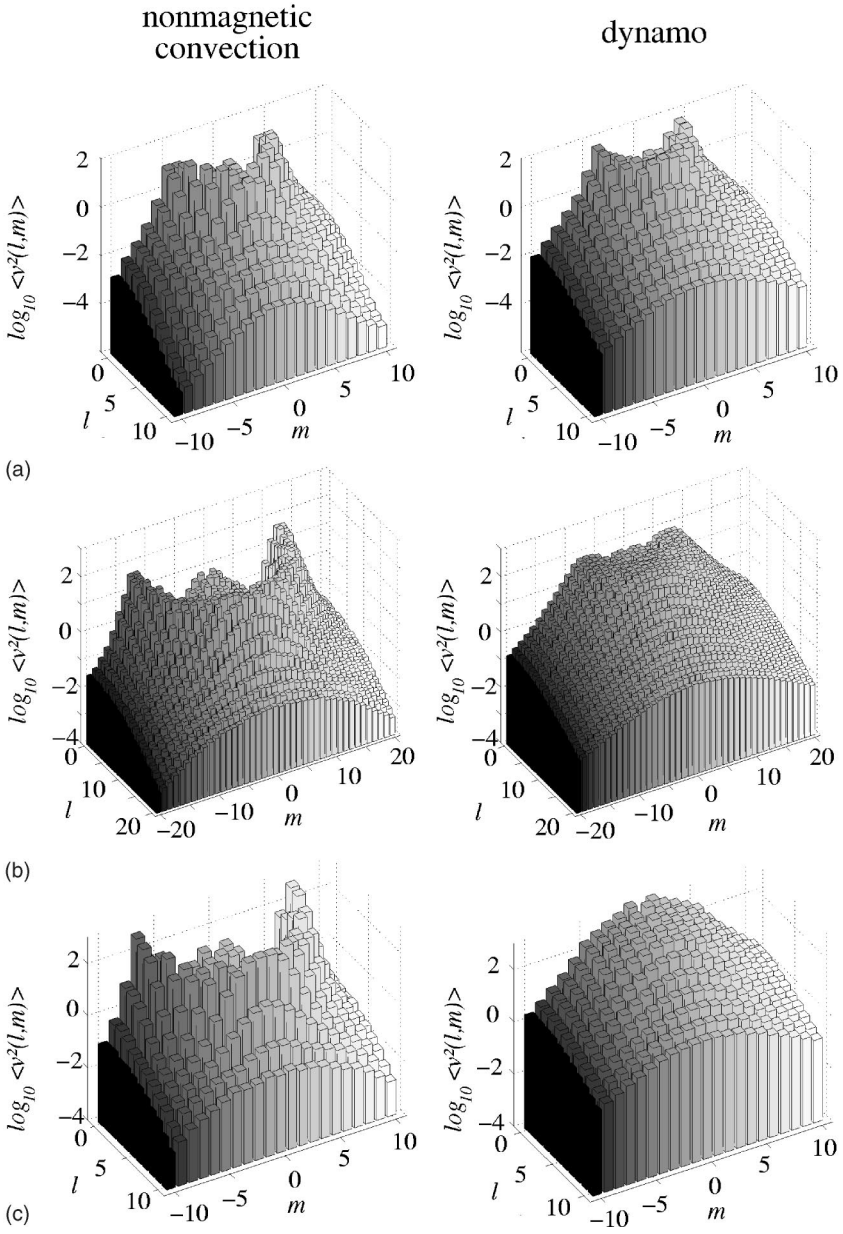

FIG. 8. Kinetic energy spectra for nonmagnetic convection (left column) and for dynamos (right column) for different values of E. The upper row (a) corresponds to $E=10^{-4}$ (run 1), the middle row (b) to $E=5\times10^{-6}$ (run 6), and the lowermost row (c) to $E=5\times10^{-7}$ (run 11).

the dynamo and the nonmagnetic spectrum. Only the distribution of the energy among modes with $k\approx k_c$ is slightly changed. For $E=5\times10^{-6}$, the spatial scales of the dynamo are already larger as compared to the nonmagnetic case and the sharp peaks at high wave numbers of order k_c almost disappear. The kinetic energy is mainly distributed among modes with wave numbers $k\leqslant9$ in contrast to the nonmagnetic case where the strongest modes have wave numbers $11\leqslant k\leqslant14$. For the lowest Ekman number considered, $E=5\times10^{-7}$, the strongest modes have $k=O(1)$ in the dynamo case and the spectrum monotonically decreases with increasing k. It has to be recalled here that in this case the computational domain has a small aspect ratio $\Gamma=0.25$. The maximum size of the convection cells is thus limited. We conclude from these results that the scale disparities between nonmagnetic and dynamo states strongly increase with decreasing Ekman number.

Figure 9 shows snapshots of the flow at $E=5\times10^{-7}$. Arrows which are scaled by the local flow speed illustrate the velocity field at the upper boundary $z=1$. The graph in the middle shows the time history of the Elsasser number and the dashed lines indicate the time instants at which the different snapshots have been taken. For comparison, the nonmagnetic case is shown in the upper left panel.

The nonmagnetic flow has the same structure as the solutions discussed in Sec. III A. In the dynamo case, quite distinct flow patterns develop at low Ekman number. On time average the flow is dominated by large scale convection. A detailed inspection of the temporal behavior reveals that strong large scale flows develop during episodes of intense magnetic field while smaller convection cells arise during times of low field intensity.

As is to be expected from the magnetoconvection results, a sufficiently strong magnetic field permits vigorous large

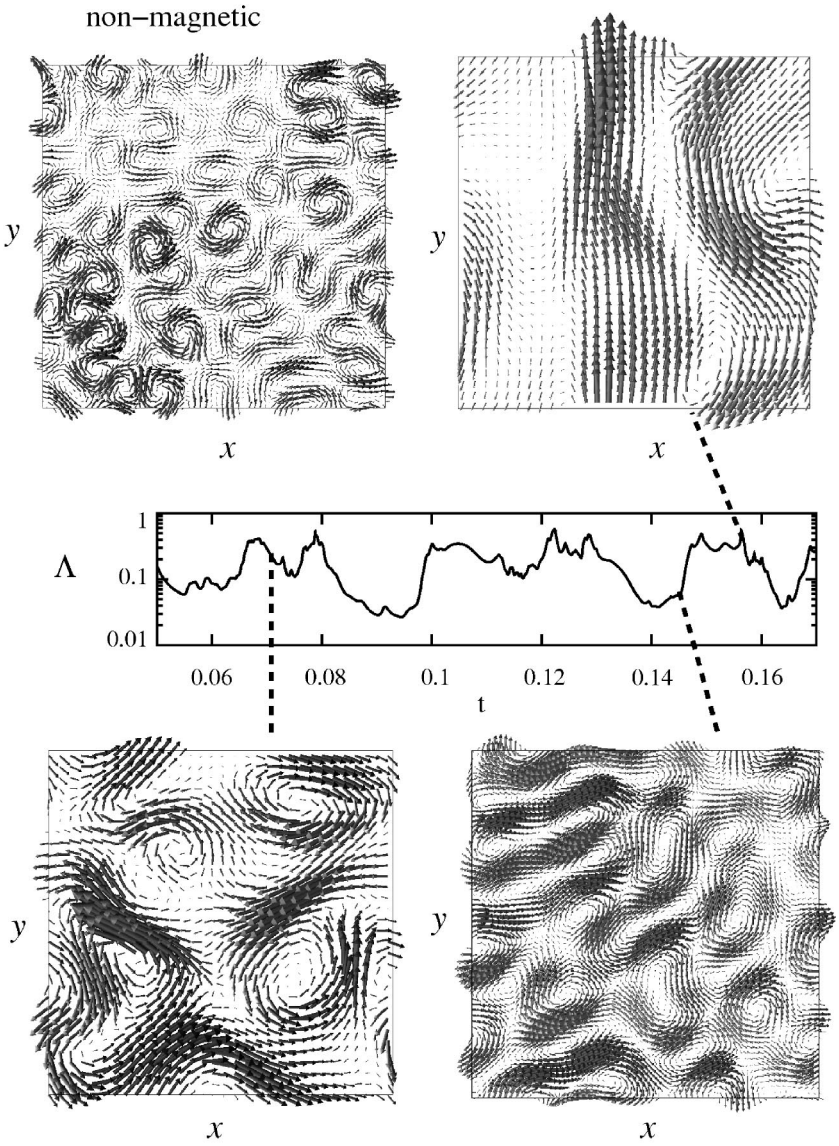

FIG. 9. Velocity field at the upper boundary $z=1$ for $E=5\times10^{-7}$, Ra $=1200$, Pr$=q=1$ at different time instants. The arrows are scaled by the local flow speed $|\mathbf{u}|$.

scale convection which efficiently transports heat across the layer. The resulting flow is, however, incapable of sustaining the strong field over long times. In contrast to the relatively ordered spatial structure which makes the nonmagnetic flow such an efficient and simple kinematic dynamo, much less regular and strongly time dependent flow patterns arise. The associated magnetic field amplitude fluctuates strongly. During times of weak field intensity, the large scale convection may break down entirely. The magnetic field then decays slowly while at the same time flow instabilities in the form of smaller convection cells develop. This small scale convection is inefficient in transporting heat but its regular structure again leads to an amplification of the magnetic field, ultimately making the small convection cells again unstable to large scale flows.

This intermittent behavior is not surprising. On the one hand, the magnetoconvection results show that at low Ekman number the convection responds rather sensitively to slight changes of the applied field strength. On the other hand, it is known from kinematic dynamo theory that often slight changes of the flow structure lead to strong changes in the efficiency of the dynamo process. The interplay of both effects is likely to generate a strongly time dependent, fluctuating dynamo. Based on a magnetoconvection study, a similar scenario has been proposed by Zhang and Gubbins for the spherical case [31,32]. Because of the higher numerical demands, the effect has not yet been observed in a self-consistent spherical dynamo simulation.

4. Magnetic field structure

The magnetic field exhibits a fairly regular structure for moderate Ekman numbers where the response of the convection to the fluctuating field is weak. In the low Ekman number case, due to the intermittent flow, the field structure is much less regular. As an example, Fig. 10 shows the field structure for intermediate Ekman number, $E=5\times10^{-6}$ at Ra$=600$, Pr$=q=1$. The upper left panel shows a snapshot of the magnetic energy at 20% of its maximum value. Typically, **B** is weak in the center of the layer and attains its maxima about midway between the center and the boundaries.

The distribution of magnetic energy among the horizontal modes is shown in Fig. 10(b). Most of the magnetic energy is

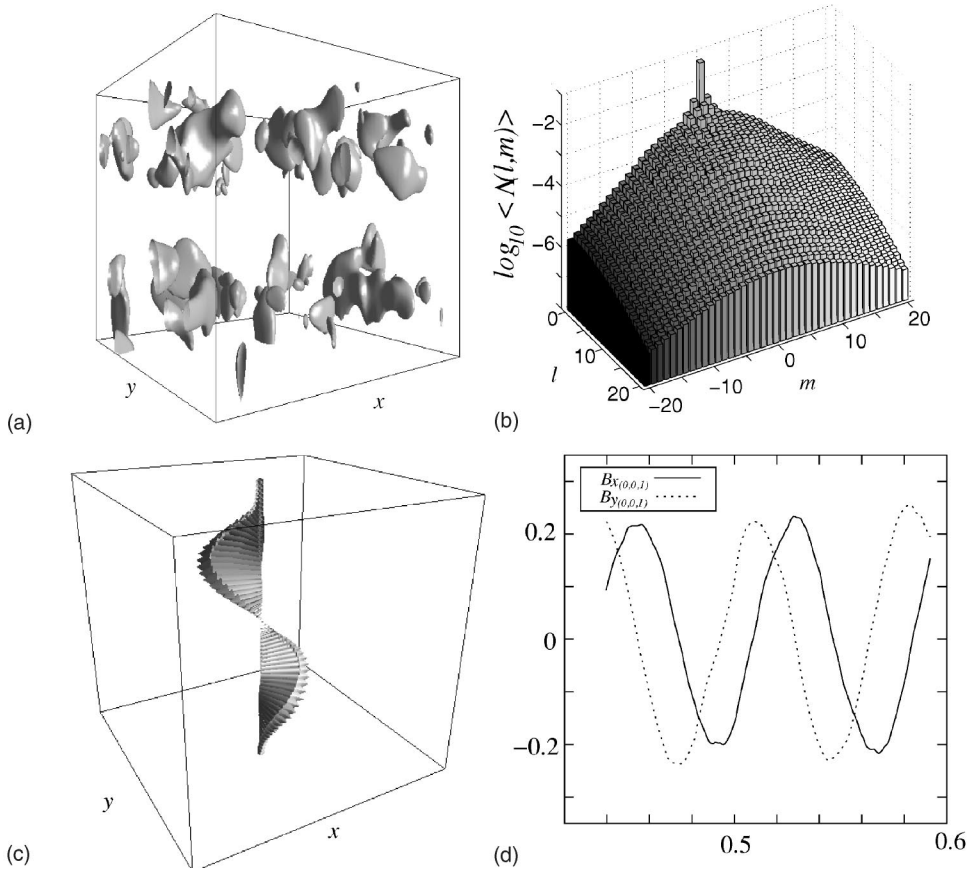

FIG. 10. Structure of the dynamo generated magnetic field at $E=5\times10^{-6}$, Ra=600, Pr=1, $q=1$. An isosurface of the magnetic energy at 20% of its maximum value is shown in (a), (b) shows the spectral distribution of the magnetic energy among the horizontal modes (see text for details), and (c) is a plot of the horizontally averaged magnetic field where the arrows are scaled by the absolute value. The time history of the Fourier coefficients $B_{x_{(0,0.1)}}$ and $B_{y_{(0,0.1)}}$ is shown in (d).

contained in the mean field modes with $(l,m)=(0,0)$. The magnetic spectrum monotonically decreases with increasing k. Small scale convection feeds energy into the high wavenumber components of the magnetic field which then moves up the spectrum in an inverse cascade.

Since the magnetic field is strongly dominated by modes with $k=0$, which play a key role in the dynamo process, we give a visualization of the mean field in Fig. 10(c). The arrows shown are scaled by its absolute value. The mean field is nearly antisymmetric with respect to the plane $z=0.5$ and resembles a spiral staircase twisting in the same sense as the velocity field. Together with the helicity, at $z=1/2$ the sense of twisting of the mean field changes sign. The appearance of this spiral staircase structure of $\mathbf{B}_\perp$ is predicted by the two scale analysis of Soward [23] and could perhaps be most vividly understood by picturing each half of the layer as a crude representation of a G. O. Roberts type dynamo [33].

The time evolution of the mean field is quite simple. To illustrate this, the last panel of Fig. 10 shows the temporal evolution of the (0,0,1) mode of the horizontal magnetic field. The figure is typical for the strongest mean-field modes which are primarily the odd modes. The mean field rotates in a sense opposite to $\mathbf{\Omega}$ with a period of the order of the free decay time of the system. This mean field rotation period is the fundamental time scale of the dynamo cycle.

The magnetic field structure is much less regular in the case $E=5\times10^{-7}$ discussed above where the planform of convection is largely controlled by the Lorentz forces.

5. Quantitative analysis

Quantitative results of the dynamo calculations are given in Table II. The values in parantheses correspond to the nonmagnetic state. The length of the time span over which the statistically fluctuating values have been averaged are given in units of the free magnetic decay time of the slowest decaying mode. Due to the high numerical cost at low Ekman number, these time spans become relatively short as typical for such studies (see, e.g., Ref. [34]). Still we feel that the obtained numbers reasonably illustrate the quantitative behavior.

A crucial output parameter of dynamo calculations is the Elsasser number Λ measuring the strength of the generated magnetic field. The magnetic fields produced have time averaged Elsasser numbers $\langle\Lambda\rangle$ in the approximate range [0.1,0.4]. Comparison with the magnetoconvection results at $E=5\times10^{-6}$ (see Fig. 5) indicates that this is about an order of magnitude to low to cause a transition to a Taylor state. Approximate Taylor states have been found at $E=O(10^{-5})$ in a recent study by Rotvig and Jones [34]. Differently from this study, the authors apply higher values of $\widetilde{R}$ and q, use a tilted rotation axes, entirely neglect inertia, and assume rigid, electrically insulating boundary conditions. As our results illustrate, at small Ekman number magnetic fields with Elsasser numbers lower than 1 can nevertheless have a profound effect on the amplitude and planform of convection. In the case of $E=5\times10^{-7}$, during times where the magnetic field is strong and the flow is characterized by large scale

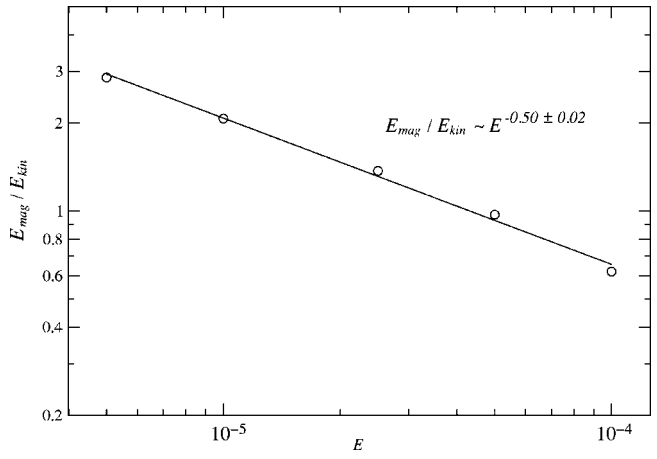

FIG. 11. Ratio of magnetic to kinetic energy as a function of the Ekman number for Pr=1, q=2.5, and constant $\widetilde{R}$.

convection, relative low values of $\tau \approx 0.1$ are observed. During times of weak magnetic fields and small scale convection, Taylor's condition is not well satisfied and higher values of τ occur.

In all cases considered, the vigor of the flow and the heat transport increases through the action of the Lorentz force. The effect is strongest in cases of relatively low magnetic Reynolds numbers and decreases for magnetic Reynolds number well beyond the critical value for the onset of dynamo action. Again, the effect manifests itself most clearly in the case $E=5\times10^{-7}$ during times where the magnetic field is strong and large scale convection very efficiently carries heat across the layer.

The ratio of magnetic to kinetic energy as a function of the Ekman number for q=2.5, Pr=1 and constant $\widetilde{R}$ (runs 1–5) is shown in Fig. 11. E_{mag}/E_{kin} increases with decreasing Ekman number approximately according to $E_{mag}/E_{kin} \propto E^{-1/2}$. If it is assumed that the Elsasser number is independent of the Ekman number and the kinetic energy scales according to $E^{-2/3}$ as in the nonmagnetic case, $E_{mag}/E_{kin} = E^{-1}(q\mathrm{Pr})\Lambda/\mathrm{Re}_m^2 \propto E^{-1/3}$. The ratio of magnetic to kinetic energy thus increases rather rapidly with decreasing E, again reflecting the fact that the convection promoting effect decreases at high magnetic Reynolds number. The absolute value of E_{mag}/E_{kin} strongly depends on the value of the Prandtl number (see run 6, 9, and 10). For high $\mathrm{Pr} \geqslant 10$, the ratio is approximately proportional to Pr. This suggests that the system becomes independent of inertia [35], since in our scaling the Prandtl number only appears in the inertia term.

6. Subcritical dynamo action

The calculations presented above clearly show that the magnetic field acts to promote convection. This gives ground to the assumption that dynamo action might also exist for lower values of the Rayleigh number, perhaps even for Rayleigh numbers below the critical value for the onset of nonmagnetic convection. Indeed, indications for subcritical dynamo action have been found in a study by St. Pierre in a parameter regime comparable to the present study [36]. His study covered only a small fraction of a mean field decay time and was confined to a periodic box of small aspect ratio. We thus find it worthwhile to reconsider the problem of subcritical dynamos here. Since an infinite time series would be necessary to safely conclude that a specific dynamo solution survives as a subcritical dynamo, we use the term "long living dynamos" for solutions which survive for the entire calculated time series which has to cover several mean field decay times of the system and avoid the term "stable" here.

Starting from the dynamo solution at $E=5\times10^{-6}$, Ra =600, Pr=q=1, we successively reduced the Rayleigh number. At Ra=500, which is only slightly below the critical value, we find a long living dynamo that survived for the entire calculated time series which covered nearly eight mean field decay times. Figure 12(a) shows the temporal evolution of the Elsasser number and of the magnetic Reynolds number. By switching off the Lorentz force in the momentum equation, we observed that convection rapidly breaks down. We therefore conclude that it is really the Lorentz force and not the nonlinear properties of the momentum equation that allow for convection and dynamo action in this case.

Encouraged by this result and the promisingly high value of the magnetic Reynolds number which fluctuates about $R_m \approx 100$ for Ra=500, we further reduced the Rayleigh number to Ra=450. Figure 12(b) again shows a plot of Λ and R_m versus time. After a short transient, the dynamo settles into a state where at first R_m fluctuates about 80 and the magnetic field shows no sign of decay. After more than two mean field decay times, however, both field and flow suddenly break down.

This clearly illustrates the difficulties in establishing subcritical dynamo action. The basin of attraction of the dynamo branch is limited and sufficiently strong fluctuations may drive the dynamo into a decay state even after a long period of apparently "stable" dynamo action. Very long time series are thus needed to conclude with high probability that a promising looking system is indeed a stable dynamo. We conclude from these results that long living subcritical dynamos exist at $E=5\times10^{-6}$, but that this subcritical branch does not extend very far into the low Rayleigh number parameter space.

IV. SUMMARY AND CONCLUDING REMARKS

In this study we aim at a better understanding of the dynamo process at low Ekman number. Cartesian models are well suited for this purpose since the simpler geometry allows to reach more extreme parameter values. Furthermore, the simplicity of the model helps us to understand the obtained results.

In order to put the interpretation of the dynamos on a firm footing, nonmagnetic convection as well as magnetoconvection with an applied mean field are studied first. The choice of a moderate value of the Rayleigh number guarantees that the nonmagnetic problem can still be interpreted on the grounds of weakly nonliner theory. The flow consists of vertical convection columns with a characteristic horizontal length scale $\mathcal{L} \propto E^{1/3}$. For fixed $(\mathrm{Ra}-\mathrm{Ra}_c)/\mathrm{Ra}_c$, the heat transport remains almost independent of the Ekman number.

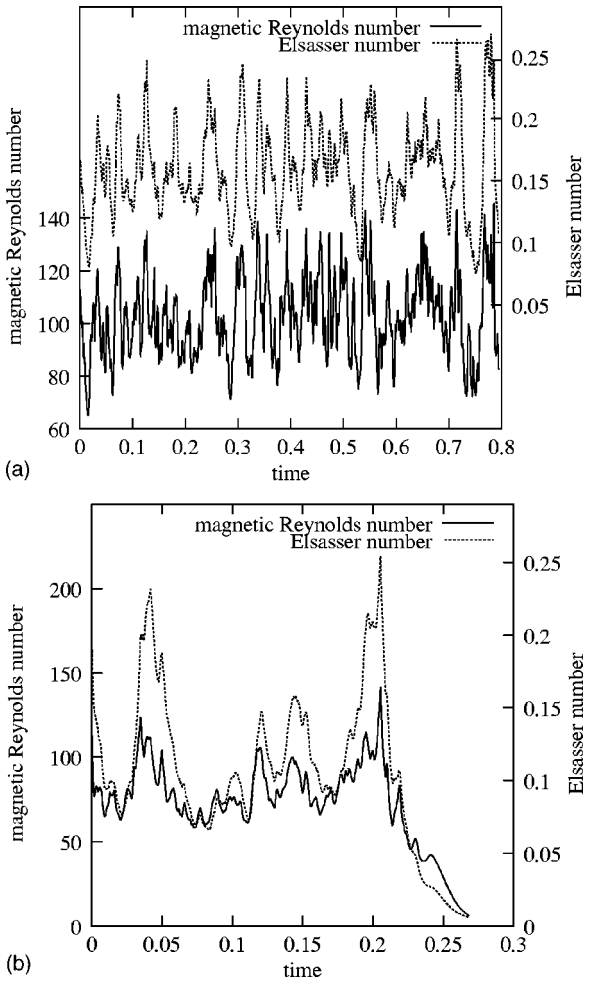

FIG. 12. Time history of the magnetic Reynolds number and of the Elsasser number for $E=5\times10^{-6}$, Pr=1, $q=1$, and (a) Ra=500, (b) Ra=450.

In contrast, the amplitude of convection as measured by its Reynolds number increases with decreasing Ekman number according to $\mathrm{Re}\propto E^{-1/3}$.

The magnetoconvection problem was addressed for the same values of the control parameters. As indicated by linear theory [24–26], we found that a drastic transition to large scale convection occurs when a sufficiently strong magnetic field is externally applied. This transition is accompanied by a strong increase of the flow amplitude and of the heat transport. For sufficiently strong imposed fields, approximate Taylor states are observed. As expected, Taylor's condition is increasingly well fullfilled with decreasing Ekman number.

The results gained in the nonmagnetic case and for the magnetoconvection problem provide the background for an understanding of the dynamo case. Our dynamo simulations reveal that with decreasing Ekman number, a transition takes place from a viscously dominated flow regime characterized by the weak field scaling $\mathcal{L}\propto E^{1/3}$ to a regime where the Lorentz forces control the flow structure to a large extend. In this regime, on time average the convective flow is dominated by long wavelength modes. The scale disparities between nonmagnetic and dynamo states strongly increase with decreasing Ekman number.

At low Ekman number, the flow reacts quite sensitively to changes of the fluctuating magnetic field. Both the amplitude and the structure of convection strongly depend on the field strength. On time average, the flow is dominated by long wavelength modes. This does not mean that small scales never dominate. As the magnetic field strength fluctuates, small convection cells develop during times of low field intensity. This small scale flow again amplifies the magnetic field by the well known two scale mechanism, and, as the field grows again, the small convection cells in turn become unstable to large scale flows. The dynamo oscillates between both states, each one being unstable to the other. This kind of behavior has been proposed to be relevant for the geodynamo by Zhang and Gubbins [31] on the basis of results from kinematic dynamo theory and from magnetoconvection.

For the moderate values of the Rayleigh number considered here, the magnetic field facilitates convection leading to phenomena like nonexponential "runaway" field growth and subcritical dynamo action. The convection promoting effect, however, seems to decrease with increasing magnetic Reynolds number. We therefore conclude that the effect might not be a robust feature at high Rayleigh number.

An important goal of dynamo modeling is a thorough understanding of the dynamics of the Earth's core. Differently from the Cartesian model studied in this paper, spherical models provide a much more realistic geometry and allow a detailed comparison of the simulations with observational data. The more complicated spherical geometry, however, permits dynamo calculations only at moderate Ekman numbers where viscous effects prevent drastic changes of the flow in response to the generated magnetic field. The behavior of spherical dynamos at low Ekman numbers is thus unknown at present time. Results for nonmagnetic convection and for magnetoconvection in spherical shells (see, e.g., Ref. [32]), however, suggest a scenario similar to the one discussed in the present paper for the Cartesian case. We therefore feel that our results are relevant for a better understanding of core dynamics.

APPENDIX: RESOLUTION

The results presented in this paper, especially the spectra shown in Fig. 8 with high frequency components being present in the calculated fields raise the question of the accurateness of these solutions. To address these issues, extensive resolution tests have been performed. For example, we interpolated our solutions at $E=5\times10^{-6}$, Ra=600, Pr=q=1 to a finer grid with twice the resolution in the horizontal direction ($256\times256\times128$ grid) and continued the calculation. To address the effects of fairly poor resolution, a solution on a 64^3 grid has also been computed. Figure 13 shows kinetic energy spectra from these calculations. Since we use time averaged spectra with $|l|,|m|\leqslant20$ as an indicator for the lowest order flow structures, we also show the corresponding diagram here.

Comparing the time averaged spectra clearly indicates that even the calculation on the very coarse 64^3 grid reveals the dominating features quite well. This is also true for the

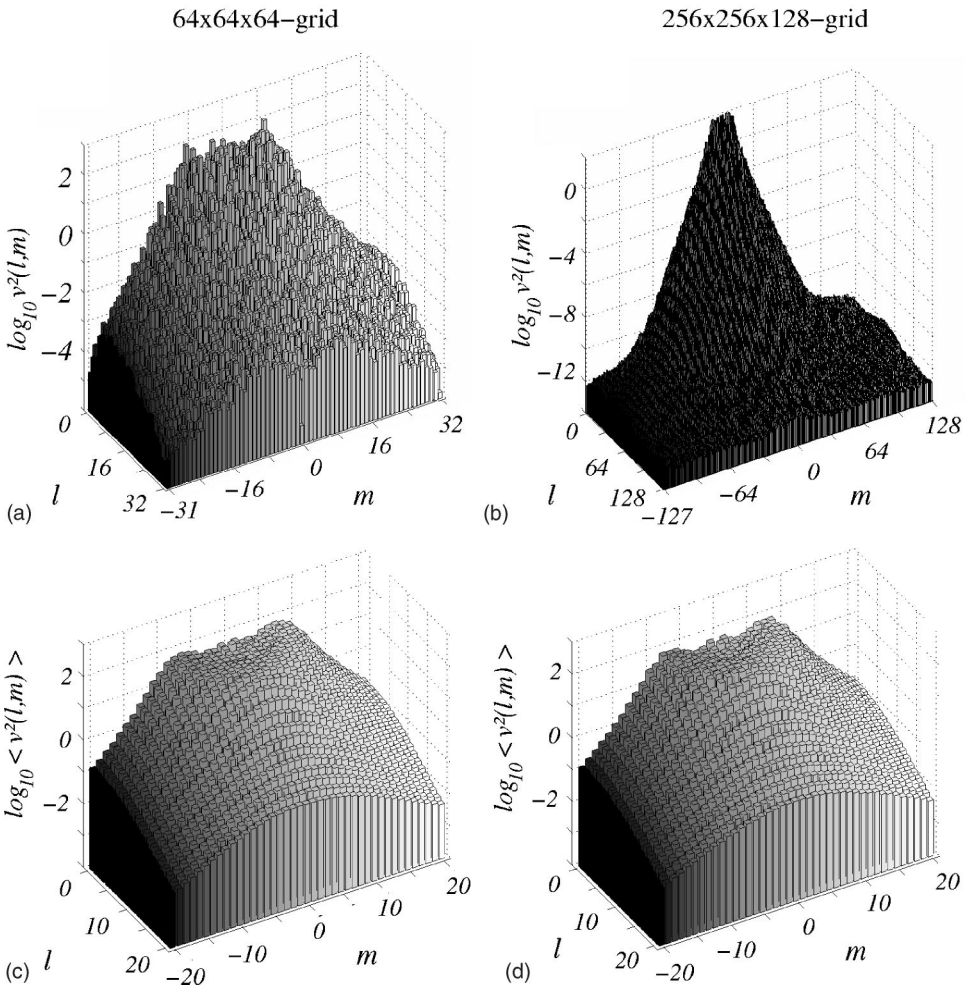

FIG. 13. Kinetic energy spectra for different resolutions at $E=5\times10^{-6}$, Pr=1, q=1, and Ra=600. Snapshots of the spectra are shown in (a) and (b) while (c) and (d) show time averaged spectra.

time averaged spectrum of the magnetic field. In addition, we reproduced the nonexponential field growth on the coarse 64^3 grid and on the fine $256\times256\times128$ grid. We thus usually choose the 128^3 grid at $E=5\times10^{-6}$ and resolutions which provide a comparable accuracy for the other Ekman numbers considered as a compromise between the conflicting demands of high accuracy and available computational resources.

ACKNOWLEDGMENTS

We gratefully acknowledge support through a grant from the Deutsche Forschungsgemeinschaft (Grant No. Ha 1765/7). Some of the calculations presented were performed on the CRAY T3E and on the JUMP cluster of the NIC Supercomputer center in Jülich. We thank Jörg Schmalzl for his support of the visualization of the calculated data.

[1] E. Dormy, J. Valet, and V. Courtillot, Geochem. Geophys. Geosyst. 1, Paper No. 2000GC000062 (2000).
[2] M. Kono and P. Roberts, Rev. Geophys. **40**, 4 (2002).
[3] G. Glatzmaier and P. Roberts, Nature (London) **377**, 203 (1995).
[4] C. Kutzner and U. Christensen, Phys. Earth Planet. Inter. **131**, 29 (2002).
[5] J. Wicht, Phys. Earth Planet. Inter. **132**, 281 (2002).
[6] M. Walker, C. Barenghi, and C. Jones, Geophys. Astrophys. Fluid Dyn. **88**, 261 (1998).
[7] S. Childress and A. Soward, Phys. Rev. Lett. **29**, 837 (1972).
[8] K. Zhang and C. Jones, Geophys. Res. Lett. **24**, 2869 (1997).
[9] E. Grote, F. Busse, and A. Tilgner, Geophys. Res. Lett. **27**, 2001 (2000).
[10] R. Hollerbach, in *Earth's Core: Dynamics, Structure, Rotation* (American Geophysical Union, Washington, D.C., 2003), pp. 181–192.
[11] G. Glatzmaier, J. Comput. Phys. **55**, 461 (1984).
[12] I. Foster, *Designing and Building Parallel Programs* (Addison-Wesley, Reading, MA, 1995).
[13] J. Schmalzl and U. Hansen, Phys. Earth Planet. Inter. **120**, 339 (2000).
[14] H. Harder and U. Hansen (unpublished).
[15] W. Elsasser, Phys. Rev. **79**, 183 (1950).

[16] B. Leonard, Comput. Methods Appl. Mech. Eng. **19**, 59 (1979).
[17] P. Wesseling, *Principles of Computational Fluid Dynamics* (Springer, Berlin, 2001).
[18] M. St. Pierre, Geophys. Astrophys. Fluid Dyn. **67**, 99 (1992).
[19] S. Patankar, *Numerical Heat Transfer and Fluid Flow* (McGraw-Hill, New York, 1980).
[20] H. A. Van Der Vorst, SIAM (Soc. Ind. Appl. Math.) J. Sci. Stat. Comput. **13**, 631 (1992).
[21] D. Gubbins, in *Geomagnetism*, edited by J. Jacobs, (Academic Press, London, 1987), pp. 1–177.
[22] S. Chandrasekhar, *Hydrodynamic and Hydromagnetic Stability* (Clarendon Press, Oxford, 1961).
[23] A. Soward, Philos. Trans. R. Soc. London, Ser. A **275**, 611 (1974).
[24] I. Eltayeb, Proc. R. Soc. London, Ser. A **326**, 229 (1972).
[25] I. Eltayeb, J. Fluid Mech. **71**, 161 (1975).
[26] P. Roberts and C. Jones, Geophys. Astrophys. Fluid Dyn. **92**, 289 (2000).
[27] C. Jones and P. Roberts, J. Fluid Mech. **404**, 311 (2000).
[28] P. Roberts and K. Stewartson, Proc. R. Soc. London, Ser. A **277**, 287 (1974).
[29] P. Roberts and K. Stewartson, J. Fluid Mech. **68**, 447 (1975).
[30] Y. Fautrelle and S. Childress, Geophys. Astrophys. Fluid Dyn. **22**, 235 (1982).
[31] K. Zhang and D. Gubbins, Geophys. J. Int. **140**, F1 (2000).
[32] K. Zhang and D. Gubbins, Philos. Trans. R. Soc. London, Ser. A **358**, 899 (2000).
[33] G. Roberts, Philos. Trans. R. Soc. London, Ser. A **271**, 411 (1972).
[34] J. Rotvig and C. Jones, Phys. Rev. E **66**, 056308 (2002).
[35] F. Busse, E. Grote, and A. Tilgner, Stud. Geophys. Geod. **42**, 211 (1998).
[36] M. St. Pierre, in *Solar and Planetary Dynamos*, edited by M. Proctor, P. Matthews, and A. Rucklidge (Cambridge University Press, Cambridge, England, 1993), pp. 295–302.